

ECOLE POLYTECHNIQUE

CENTRE DE MATHÉMATIQUES APPLIQUÉES

UMR CNRS 7641

91128 PALAISEAU CEDEX (FRANCE). Tél: 01 69 33 46 00. Fax: 01 69 33 46 46
<http://www.cmap.polytechnique.fr/>

**A level set method for the
numerical simulation of damage
evolution**

Grégoire Allaire, François Jouve,
Nicolas Van Goethem

R.I. 629

December 2007

A LEVEL SET METHOD FOR THE NUMERICAL SIMULATION OF DAMAGE EVOLUTION

GRÉGOIRE ALLAIRE¹, FRANÇOIS JOUVE², AND NICOLAS VAN GOETHEM³

ABSTRACT. This paper is devoted to the numerical simulation of the evolution of damage in brittle materials following the Francfort-Marigo model. This model is based on a Griffith energy criterion for the competition between the two phases, healthy and damaged, separated by a sharp interface. In a quasi-static and irreversible framework, the damage configuration is obtained by minimizing a total energy using a gradient descent method. The interface is modeled by a level set function which is advected by the energy gradient issued from a shape derivation. The nucleation of the damaged zone is obtained by using the so-called topological derivative. Several numerical examples in 2-d and 3-d are discussed.

¹ Centre de Mathématiques Appliquées, École Polytechnique, 91128 Palaiseau, France.

Email: gregoire.allaire@polytechnique.fr

² Laboratoire J.L.Lions, Université Paris 7 - Denis Diderot, 75252 Paris, France.

Email: jouve@math.jussieu.fr

³ Centre de Mathématiques Appliquées, École Polytechnique, 91128 Palaiseau, France.

Email: vangoeth@cmap.polytechnique.fr

1. INTRODUCTION AND MODEL

This work is concerned with the Francfort-Marigo model [15] of quasi-static damage evolution for brittle materials. In a body $\Omega \in \mathbb{R}^d$ ($d = 2, 3$) the damage problem is stated as a macroscopic phase transition model, the first phase being the undamaged, otherwise called “healthy” phase, while the second phase is the damaged one. The damaged zone is denoted by $\Omega^0 \subset \Omega$, while the healthy zone is the remaining region $\Omega^1 = \Omega \setminus \Omega^0$. The characteristic function of Ω^0 is denoted by χ . Both the healthy and damaged phases are assumed to be linear, isotropic and homogeneous, so we work in a linearized elasticity framework and the Lamé tensor of elasticity in Ω is

$$A_\chi = A^1(1 - \chi) + A^0\chi,$$

where $0 < A^0 < A^1$ are the Lamé tensors of isotropic elasticity in the damaged and healthy regions, respectively, defined by

$$A^i = 2\mu^i I_4 + \lambda^i I_2 \otimes I_2$$

with $i = 0, 1$. Recall that, in space dimension d , the Young modulus E and the Poisson ratio ν are related to the Lamé moduli by $\lambda = \frac{E\nu}{(1+\nu)(1+(1-d)\nu)}$ and $\mu = \frac{E}{2(1+\nu)}$.

This work has been supported by the MULTIMAT european network MRTN-CT-2004-505226 funded by the EEC. G. Allaire was also partly supported by the GdR MoMaS CNRS-2439 sponsored by ANDRA, BRGM, CEA, EDF, and IRSN. .

The boundary of the body is made of two parts, $\partial\Omega = \Gamma_D \cup \Gamma_N$, where a Dirichlet boundary condition is imposed on Γ_D and a Neumann boundary condition is imposed on Γ_N . We denote by n the normal unit vector on $\partial\Omega$. We introduce the space of admissible displacement fields

$$V = \{u \in H^1(\Omega, \mathbb{R}^d) \text{ such that } u = 0 \text{ on } \Gamma_D\}.$$

As usual, the strain and stress tensors write as

$$(1) \quad e(u) = \frac{1}{2} (\nabla u + \nabla^T u), \quad \sigma(u) = Ae(u).$$

For given body and surface loads f and g , the elasticity system is

$$(2) \quad \begin{cases} -\operatorname{div}(A_\chi e(u_\chi)) = f & \text{in } \Omega \\ u_\chi = 0 & \text{on } \Gamma_D \\ A_\chi e(u_\chi)n = g & \text{on } \Gamma_N \end{cases}$$

It is well-known that (2) can be restated as a minimum potential energy principle, that is, the displacement field $u_\chi \in V$ minimizes in V the energy functional

$$\mathcal{P}_\chi(u) = \int_\Omega \left(\frac{1}{2} A_\chi e(u) \cdot e(u) - f \cdot u \right) dV - \int_{\Gamma_N} g \cdot u dS.$$

The Francfort-Marigo model consists in a global combined minimization over u and χ of the potential energy functional to which a Griffith energy for the creation of the damaged region is added, writing as

$$\int_{\Omega^0} \kappa dV,$$

where κ is known as the Griffith's energy release rate. In other words, the Francfort-Marigo model is based on the minimization of

$$(3) \quad \mathcal{J}(u, \chi) = \int_\Omega \left(\frac{1}{2} A_\chi e(u) \cdot e(u) + \kappa \chi - f \cdot u \right) dV - \int_{\Gamma_N} g \cdot u dS.$$

Since the latter is a min – min problem, and since the displacement field u_χ identically satisfies

$$\int_\Omega A_\chi e(u_\chi) \cdot e(u_\chi) dV = \int_\Omega f \cdot u_\chi dV + \int_{\Gamma_N} g \cdot u_\chi dS,$$

the cost function to be minimized reads

$$(4) \quad J(\chi) = \mathcal{J}(u_\chi, \chi) = \int_\Omega \left(-\frac{1}{2} A_\chi e(u_\chi) \cdot e(u_\chi) + \kappa \chi \right) dV.$$

It results from this global minimization, that at a point $x \in \Omega$, the choice for phase 0 or 1 is made according to the following local minimization

$$\min_{\chi \in \{0,1\}} \left\{ \frac{1}{2} A_\chi e(u_\chi) \cdot e(u_\chi) + \kappa \chi \right\}(x),$$

providing a transition from the healthy to the damaged phase as soon as the release of elastic energy is larger than the threshold κ , namely if

$$(5) \quad A^1 e(u_\chi) \cdot e(u_\chi) - A^0 e(u_\chi) \cdot e(u_\chi) \geq \kappa.$$

The model is quasi-static which means that the time is discretized by an increasing sequence $(t_i)_{i \geq 0}$, with $t_0 = 0$ and $t_i < t_{i+1}$. At each time t_i the loads are denoted by f_i and g_i , the characteristic function of the damaged phase is χ_i and the corresponding displacement is $u_i = u_{\chi_i}$, solution of (2) with loads f_i and g_i .

The model is irreversible which means that a material point $x \in \Omega$ which is damaged at time t_i must remain damaged at later times, i.e.,

$$(6) \quad \chi_{i+1}(x) \geq \chi_i(x).$$

Therefore, introducing \mathcal{J}_i and J_i , which are defined as (3) and (4) with the loads at time t_i , the Francfort-Marigo model is a sequence, indexed by $i \geq 0$, of minimization problems

$$(7) \quad \min_{\chi \in L^\infty(\Omega; \{0,1\}), \chi \geq \chi_{i-1}} J_i(\chi) = \int_{\Omega} \left(-\frac{1}{2} A_\chi e(u_\chi) \cdot e(u_\chi) + \kappa \chi \right) dV,$$

or equivalently, using (3),

$$\min_{u \in V, \chi \in L^\infty(\Omega; \{0,1\}), \chi \geq \chi_{i-1}} \mathcal{J}_i(u, \chi),$$

with minimizers χ_i and u_i .

In the original work of Francfort and Marigo [15] and in the subsequent refinements [14], [18], a global solution to the variational problem (7) is sought. This is at the root of mathematical and mechanical difficulties. First of all, the existence of minimizers for (7) is not always guaranteed. Actually, the relaxation of (7) was given in [15] which proved that the optimal solution can be a mixture of phase 0 and 1 (a composite material) instead of a macroscopic spatial distribution of these two pure phases. Secondly, the use of a global minimization process can yield damage, at time step t_{i+1} , in a region far away from the previous damaged region at time step t_i , whereas it seems more sensible from a physical viewpoint to have expansion of the previously damaged zone. Therefore, it might be reasonable to use local minimizers in (7) which may avoid these two inconveniences of global minimizers. However, the definition of local minimizers strongly depend on the chosen topology and there is no clear and unambiguous choice.

The goal of our work is to numerically investigate the Francfort-Marigo model and to consider local minimizers in the framework of the Hadamard method of shape optimization (see [1], [19] and references therein). In other words, we parametrize the characteristic function χ by the interface between the healthy and damaged zone. This surface is moved with a normal velocity which is a descent direction for the cost functional (7), computed by shape differentiation. Since we use a simple steepest descent gradient algorithm, we compute local minimizers which may be not global. Here, local has to be understood in the topology of diffeomorphisms parameterizing the interface. The irreversibility constraint is taken into account by adding to the predicted damaged zone the previously damaged region so that it never decreases.

From a numerical standpoint, the interface between the healthy and damaged subdomains is captured by using the level set method of Osher and Sethian [21] in a way very similar to what is done in structural optimization [3]. In section 2 we give the shape derivative of (7). It turns out that this sole notion of shape derivative is not sufficient for nucleating a damaged zone in an entire healthy domain. Therefore, in section 3 we recall the notion of topological derivative, as introduced in [13], [17], [23], and applied to the case of elastic inclusions in [7], [8]. The topological derivative indicates where it might be energetically interesting to nucleate an infinitesimal damage inclusion in the healthy region. Eventually section 4 is devoted to various numerical experiments. We do not give complete proofs of our results neither do

we make exhaustive numerical experiments. Instead we refer to our future more complete work [5].

2. COMPUTATION OF THE SHAPE GRADIENT

The goal of this section is to compute the shape derivative of the cost function (4), following the well-known Hadamard method (see e.g. [1], [19] and references therein). This shape derivative will serve as an advection velocity for the boundary of the damaged zone when numerically minimizing (4). Throughout this section we assume that the sets Ω, Ω^0 and Ω^1 have smooth boundaries, and that the loads f and g are smooth functions from Ω into \mathbb{R}^d . We also drop the index i , denoting the time step, for notational simplicity.

The total body Ω is fixed in our problem. Rather, the subdomains Ω^0 and Ω^1 (or equivalently their interface Σ) are varying. Therefore, it makes sense to rewrite u_χ , solution of (2), in terms of its restrictions u^0 and u^1 in Ω^0 and Ω^1 , respectively, which satisfy

$$(8) \quad \begin{cases} -\operatorname{div} A^1 e(u^1) = f & \text{in } \Omega^1 \\ u^1 = 0 & \text{on } \Gamma_D^1 = \Gamma_D \cap \partial\Omega^1 \\ A^1 e(u^1) n^1 = g & \text{on } \Gamma_N^1 = \Gamma_N \cap \partial\Omega^1 \\ u^1 = u^0 & \text{on } \Sigma = \partial\Omega^0 \cap \partial\Omega^1 \\ A^1 e(u^1) n^1 + A^0 e(u^0) n^0 = 0 & \text{on } \Sigma \end{cases}$$

and

$$(9) \quad \begin{cases} -\operatorname{div} A^0 e(u^0) = f & \text{in } \Omega^0 \\ u^0 = 0 & \text{on } \Gamma_D^0 = \Gamma_D \cap \partial\Omega^0 \\ A^0 e(u^0) n^0 = g & \text{on } \Gamma_N^0 = \Gamma_N \cap \partial\Omega^0 \\ u^0 = u^1 & \text{on } \Sigma = \partial\Omega^0 \cap \partial\Omega^1 \\ A^0 e(u^0) n^0 + A^1 e(u^1) n^1 = 0 & \text{on } \Sigma \end{cases}$$

In the sequel, we simply denote by $n = n^0 = -n^1$ the unit normal vector to Σ . Similarly, the cost function (4) can be rewritten

$$(10) \quad \begin{aligned} J(\chi) = & \int_{\Omega^0} \left(-\frac{1}{2} f \cdot u^0 + \kappa \right) dV - \int_{\Omega^1} \frac{1}{2} f \cdot u^1 dV \\ & - \frac{1}{2} \int_{\Gamma_N^0} g \cdot u^0 dS - \frac{1}{2} \int_{\Gamma_N^1} g \cdot u^1 dS, \end{aligned}$$

where u^0 and u^1 are the solutions of (8)-(9). The corresponding Lagrangian (i.e. the sum of the cost function (10) and of the variational formulation for (8)-(9) seen as constraints) reads

$$(11) \quad \begin{aligned} \mathcal{L}(v^1, v^0, p^1, p^0, \chi) = & \int_{\Omega^0} \kappa dV \\ & - \int_{\Omega^1} \left[A^1 e(v^1) \cdot e(p^1) + f \cdot \left(\frac{1}{2} v^1 - p^1 \right) \right] dV + \int_{\Gamma_N^1} g \cdot \left(p^1 - \frac{1}{2} v^1 \right) dS \\ & - \int_{\Omega^0} \left[A^0 e(v^0) \cdot e(p^0) + f \cdot \left(\frac{1}{2} v^0 - p^0 \right) \right] dV + \int_{\Gamma_N^0} g \cdot \left(p^0 - \frac{1}{2} v^0 \right) dS \\ & - \frac{1}{2} \int_{\Sigma} (A^1 e(v^1) + A^0 e(v^0)) n \cdot (p^1 - p^0) dS \\ & - \frac{1}{2} \int_{\Sigma} (A^1 e(p^1) + A^0 e(p^0)) n \cdot (v^1 - v^0) dS \end{aligned}$$

where p^0 and p^1 play the role of Lagrange multiplier or, at optimality, of the adjoint state (on the same token, at optimality v^0, v^1 are equal to u^0, u^1). All functions v^0, v^1, p^0, p^1 belong to the space V which implies that they satisfy a homogeneous Dirichlet boundary condition on Γ_D .

In order to apply a gradient method to the minimization of (10) we recall the classical notion of shape derivative. Starting from a characteristic function χ of a smooth reference subdomain Ω^0 , we consider variations of the type

$$\chi_\theta = \chi \circ (Id + \theta), \text{ i.e., } \chi_\theta(x) = \chi(x + \theta(x)),$$

with $\theta \in W^{1,\infty}(\mathbb{R}^d, \mathbb{R}^d)$ such that θ is tangential on $\partial\Omega$ (this last condition ensures that $\Omega = (Id + \theta)\Omega$). It is well known that, for sufficiently small θ , $(Id + \theta)$ is a diffeomorphism in \mathbb{R}^d .

Definition 2.1. *The shape derivative of a function $J(\chi)$ at χ is defined as the Fréchet derivative in $W^{1,\infty}(\mathbb{R}^d, \mathbb{R}^d)$ at 0 of the application $\theta \rightarrow J(\chi \circ (Id + \theta))$, i.e.*

$$J(\chi \circ (Id + \theta)) = J(\chi) + J'(\chi)(\theta) + o(\theta) \quad \text{with} \quad \lim_{\theta \rightarrow 0} \frac{|o(\theta)|}{\|\theta\|} = 0,$$

where $J'(\chi)$ is a continuous linear form on $W^{1,\infty}(\mathbb{R}^d, \mathbb{R}^d)$.

Let us recall the following classical result.

Lemma 2.2. *Let ω be a smooth bounded open set and $\theta \in W^{1,\infty}(\mathbb{R}^d, \mathbb{R}^d)$. Let $f \in H^1(\mathbb{R}^d)$ and $g \in H^2(\mathbb{R}^d)$ be two given functions. Assume that Γ is a smooth subset of $\partial\omega$ with boundary $\gamma = \partial\Gamma$. The shape derivatives of*

$$(12) \quad J_1(\omega) = \int_{\omega} f dV \quad \text{and} \quad J_2(\omega) = \int_{\Gamma} g dS$$

are $J'_1(\omega) = \int_{\partial\omega} f\theta \cdot n dS$ and

$$J'_2(\omega) = \int_{\Gamma} \left[\frac{\partial g}{\partial n} + gH \right] \theta \cdot n dS + \int_{\gamma} g\theta \cdot \tau dl,$$

respectively, where n is the unit vector normal to $\partial\omega$, H is the mean curvature and τ is the unit vector tangent to $\partial\omega$ such that τ is normal to both γ and n , and dl is the line measure along γ .

Let us explain how to use Lemma 2.2 in order to compute the shape derivative of (10). We rely on the well-known Lagrangian approach in shape optimization problems (see, e.g., [1], [3], [22]). The Lagrangian (11) has been devised in such a way that its partial derivatives with respect to p^0 and p^1 , when equal to 0, yield the state equation (8)-(9), including the transmission boundary conditions on the interface Σ . Conversely, the partial derivatives of the Lagrangian with respect to v^0 and v^1 , when equal to 0, provide the so-called adjoint equation for p^0 and p^1 . It turns out that, due to the special choice of the cost function (10), the problem is self-adjoint, namely the optimal p^0 and p^1 are explicitly given in terms of u^0 and u^1 by $p^i = -u^i/2$.

The main interest of the Lagrangian is that its partial derivative with respect to the shape χ , evaluated at the state u_χ and adjoint p_χ , is equal to the shape derivative of the cost function

$$J'(\chi)(\theta) = \frac{\partial \mathcal{L}}{\partial \chi}(u^1, u^0, -u^1/2, -u^0/2, \chi)(\theta).$$

The notation $\frac{\partial \mathcal{L}}{\partial \chi}$ means that it is a shape partial derivative, i.e. we differentiate \mathcal{L} in the sense of Definition 2.1 while keeping the other arguments (v^1, v^0, p^1, p^0) fixed. Therefore, in order to prove Theorems 2.3 and 2.4 below, it is enough, for fixed functions (v^1, v^0, p^1, p^0) (not depending on χ), to differentiate the functional

$$\chi \rightarrow \mathcal{L}(v^1, v^0, p^1, p^0, \chi)$$

which is just a combination of volume integrals in Ω^0, Ω^1 and surface integrals on Σ (the integrals on Γ_N do not contribute to the shape derivative because Γ_N is fixed). Applying Lemma 2.2 to \mathcal{L} yields the following results.

Theorem 2.3. *In $2-d$ the shape derivative of (10) in the direction θ is*

$$\begin{aligned} J'(\chi)(\theta) &= \int_{\Sigma} \kappa \theta \cdot n \, dS \\ &+ \left[\left[\frac{1-\nu^2}{2E} \right] \int_{\Sigma} \sigma_{nn}^2(u_\chi) \theta \cdot n \, dS + \left[\left[\frac{1+\nu}{E} \right] \int_{\Sigma} \sigma_{tn}^2(u_\chi) \theta \cdot n \, dS \right. \right. \\ &\left. \left. - [\nu] \int_{\Sigma} \sigma_{nn}(u_\chi) e_{tt}(u_\chi) \theta \cdot n \, dS - \left[\left[\frac{E}{2} \right] \int_{\Sigma} e_{tt}^2(u_\chi) \theta \cdot n \, dS, \right. \right. \end{aligned}$$

where t is the tangential direction (orthogonal to n).

We use the jump notation

$$[[\alpha]] = \alpha^1 - \alpha^0$$

for a quantity α that has a jump through the interface Σ between the healthy and damaged regions.

Theorem 2.4. *In $3-d$ the shape derivative of (10) in the direction θ is*

$$\begin{aligned} J'(\chi)(\theta) &= \int_{\Sigma} \kappa \theta \cdot n \, dS + \left[\left[\frac{1+\nu}{E} \right] \int_{\Sigma} (\sigma_{1n}^2(u_\chi) + \sigma_{2n}^2(u_\chi)) \theta \cdot n \, dS \right. \\ &+ \left[\left[\frac{1-\nu-2\nu^2}{2E(1-\nu)} \right] \int_{\Sigma} \sigma_{nn}^2(u_\chi) \theta \cdot n \, dS - \left[\left[\frac{E\nu}{2(1-\nu^2)} \right] \int_{\Sigma} e_{11}(u_\chi) e_{22}(u_\chi) \theta \cdot n \, dS \right. \right. \\ &- \left[\left[\frac{\nu}{1-\nu} \right] \int_{\Sigma} \sigma_{nn}(u_\chi) (e_{11}(u_\chi) + e_{22}(u_\chi)) \theta \cdot n \, dS \right. \\ &- \left[\left[\frac{E}{2(1-\nu^2)} \right] \int_{\Sigma} (e_{11}^2(u_\chi) + e_{22}^2(u_\chi)) \theta \cdot n \, dS \right. \\ &\left. \left. - \left[\left[\frac{E}{2(1+\nu)} \right] \int_{\Sigma} e_{12}^2(u_\chi) \theta \cdot n \, dS, \right. \right. \end{aligned}$$

where the indices 1 and 2 refer to the tangential directions (orthogonal to n).

The proofs of Theorems 2.3 and 2.4 are given in [5] in a more general context. Similar results in the conductivity setting (scalar equations) appeared in [9], [20], [22].

When applying Lemma 2.2, there is a subtle difficulty in the interpretation of the results because the integrands in the integrals on Σ are not continuous through the interface Σ . Actually, only the displacement and the normal stress vector are continuous in view of the transmission conditions in (8)-(9). By continuity of the displacements and standard elliptic regularity, we can deduce that its tangential derivatives are also continuous. In other words, we rewrite all integrals on Σ in terms of continuous quantities and jumps of the elastic moduli thanks to the following lemma.

Lemma 2.5. *Let e and σ denote the strain and stress tensors of the solution to the state equation (2), which are smooth functions on both side of the interface Σ . The components σ_{nt} , σ_{nn} , $e_{tt'}$ and e_{tt} are continuous across Σ , and the other components can be rewritten in terms of these continuous quantities as*

$$\begin{cases} e_{nn} = (2\mu + \lambda)^{-1}(\sigma_{nn} - \lambda \operatorname{tre}^d) \\ e_{tn} = (2\mu)^{-1}\sigma_{tn} \\ \sigma_{tt'} = 2\mu e_{tt'} \quad \text{for } t \neq t' \\ \sigma_{tt} = 2\mu e_{tt} + \lambda(\operatorname{tre}^d + e_{nn}) = 2\mu e_{tt} + \lambda\left(\frac{2\mu}{2\mu + \lambda} \operatorname{tre}^d + (2\mu + \lambda)^{-1}\sigma_{nn}\right) \end{cases}$$

with $\operatorname{tre}^d = \sum_{i \neq n} e_{ii}$.

Proof. Recall that n is the normal unit vector of Σ and t (or t') is any tangential unit vector, orthogonal to n . These relations simply follows from the strain-stress relation (1) and

$$\sigma_{nn} = 2\mu e_{nn} + \lambda(\operatorname{tre}^d + e_{nn}) \Rightarrow (2\mu + \lambda)e_{nn} = \sigma_{nn} - \lambda \operatorname{tre}^d. \quad \square$$

3. TOPOLOGICAL DERIVATIVE

Hadamard method of shape variation is able to reproduce the growth of a pre-existing damaged zone but is unable to predict the onset of damage in a healthy structure. The topological derivative, introduced in [13], [17], [23] for the case of holes in an elastic body, and in [7], [8] for elastic inclusions, is the right tool for nucleating an infinitesimal damaged region. The coupling of topological derivative and shape gradient with the level set method is by now well understood in structural optimization [4], [12], [25] The aim of this section is to recall this notion of topological gradient.

We define an infinitesimal damaged inclusion D_ρ of size ρ centered at a point $x_0 \in \Omega^1$ in the healthy subdomain and of rescaled shape D

$$(13) \quad D_\rho = \left\{x \text{ such that } \frac{x - x_0}{\rho} \in D\right\},$$

and observe the variation of the cost function upon introduction of D_ρ . Without this inclusion the body Ω is separated in its healthy subdomain Ω^1 and its damaged subdomain Ω^0 . When adding D_ρ , the body is now partitioned as

$$\Omega = \Omega_\rho^0 \cup \Omega_\rho^1 \quad \text{with} \quad \Omega_\rho^0 = \Omega^0 \cup D_\rho,$$

where, for small enough ρ , D_ρ is disconnected from Ω^0 . We denoted by $\chi_\rho, \chi, \chi_{D_\rho}$ the characteristic functions of Ω_ρ^0, Ω^0 and D_ρ , respectively, satisfying $\chi_\rho = \chi + \chi_{D_\rho}$.

Definition 3.1. *If the objective function J admits the following so-called topological asymptotic expansion for small $\rho > 0$*

$$J(\chi_\rho) - J(\chi) - \rho^d DJ(x_0) = o(\rho^d),$$

then the number $DJ(x_0)$ is called the topological derivative of J at x_0 for the inclusion shape D .

Based on results in [6] we obtain the following lemma (see [5] for details).

Lemma 3.2. *For $x_0 \in \Omega^1$ and any shape D , the cost function $J(\chi)$, defined by (4), admits the following topological derivative*

$$DJ(x_0) = \kappa + \frac{1}{2}e(u_\chi)(x_0)Me(u_\chi)(x_0),$$

where u_χ is the solution of the state equation (2) in Ω without the inclusion D_ρ , and M is a non-positive fourth-order tensor depending only on the shape D and the phase properties A^0, A^1 .

The tensor M is called the elastic moment, or polarization, tensor. It can be computed explicitly for spherical inclusions. In $2d$, the topological derivative writes as:

$$\begin{aligned} DJ(x_0) &= \kappa + 2\pi\rho^2 \frac{\mu_1(\mu_0 - \mu_1)(\lambda_1 + 2\mu_1)}{\lambda_1(\mu_0 + \mu_1) + \mu_1(\mu_1 + 3\mu_0)} e(u) \cdot e(u) \\ &+ \frac{\pi\rho^2}{2} \left(-\frac{(\lambda_1 + 2\mu_1)(\lambda_1 + \mu_1 - \lambda_0 - \mu_0)}{\lambda_0 + \mu_0 + \mu_1} + 2\frac{\mu_1(\mu_1 - \mu_0)(\lambda_1 + 2\mu_1)}{\lambda_1(\mu_0 + \mu_1) + \mu_1(\mu_1 + 3\mu_0)} \right) (\text{tre}(u))^2. \end{aligned}$$

In $3d$, the topological derivative writes as:

$$DJ(x_0) = \kappa + \pi\rho^3 \frac{2}{3b} \left(\frac{(\lambda_1 - \lambda_0)b - 2(\mu_1 - \mu_0)a}{(3a + b)} (\text{tre}(u))^2 + 2(\mu_1 - \mu_0)e(u) \cdot e(u) \right),$$

with

$$a = \frac{\lambda_1(\mu_1 - \mu_0) - 5\mu_1\nu_1(\lambda_1 - \lambda_0)}{15\lambda_1\mu_1(1 - \nu_1)}, \quad b = \frac{-15\mu_1(1 - \nu_1) + 2(\mu_1 - \mu_0)(4 - 5\nu_1)}{15\mu_1(1 - \nu_1)},$$

$$\text{where } \nu_1 = \frac{\lambda_1}{2(\lambda_1 + \mu_1)}.$$

4. ALGORITHM AND NUMERICAL EXPERIMENTS

Our goal is to compute, for each discrete time t_i , $i \geq 0$, a minimizer χ_i of the Francfort-Marigo model (7). As we already said, we are interested in local minima. Our notion of local minima is numerical in essence, that is, we minimize (7) with a gradient descent algorithm in the level set framework. A minima is thus local in the sense of perturbations of the location of the interface Σ . Our algorithm is made of two nested loops:

- (i) an outer loop corresponding to the increasing sequence of discrete times t_i , $i \geq 0$,
- (ii) an inner loop of gradient iterations for the minimization of the functional (7) at each fixed time step t_i .

The irreversibility constraint (6) on the damaged zone is taken into account in the outer loop (i). However, the inner loop (ii) is purely numerical and is not subject to this irreversibility constraint between two successive iterates of (ii). The inner loop is performed with the level set method of Osher and Sethian [21] that we now briefly describe (it is very similar with its application in the context of shape optimization [3], [24]).

In the fixed bounded domain Ω , uniformly meshed once and for all, we parameterize the damaged zone Ω^0 by means of a level set function ψ such that

$$\begin{cases} \psi(x) = 0 & \Leftrightarrow x \in \Sigma, \\ \psi(x) < 0 & \Leftrightarrow x \in \Omega^0, \\ \psi(x) > 0 & \Leftrightarrow x \in \Omega^1. \end{cases}$$

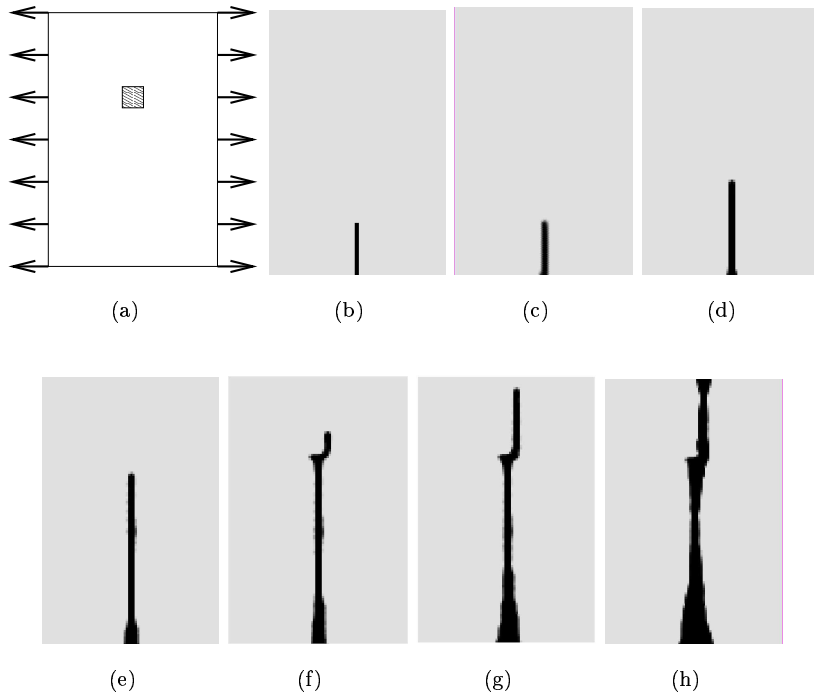


FIGURE 1. Mode I crack: boundary conditions (a), initial crack (b). Cracks for a load intensity $g = 1.2348$ (c), $g = 1.2391$ (d), $g = 1.2526$ (e), $g = 1.2751$ (f), $g = 1.2981$ (g) $g = 1.3074$ (h).

The normal n to the damaged region Ω^0 is recovered as $\nabla\psi/|\nabla\psi|$ and the curvature H is given by the divergence of the normal $\operatorname{div}n$ (these quantities are evaluated by finite differences since our mesh is uniformly rectangular). Remark that, although n and H are theoretically defined only on Σ , the level-set method allows to define easily their extension in the whole domain Ω .

Following the minimization process, the damaged zone is going to evolve according to a fictitious time s which corresponds to descent stepping and has nothing to do with the "real" time t_i in the outer loop (i). As is well-known, if the shape is evolving in time, then the evolution of the level-set function is governed by a simple Hamilton-Jacobi equation. To be precise, assume that the shape $\Omega^0(s)$ evolves according to a pseudo-time $s \in \mathbb{R}^+$ with a normal velocity $V(s, x)$. Then

$$\psi(s, x(s)) = 0 \quad \text{for any } x(s) \in \partial\Sigma(s).$$

Differentiating in s yields

$$\frac{\partial\psi}{\partial s} + \dot{x}(s) \cdot \nabla\psi = \frac{\partial\psi}{\partial s} + Vn \cdot \nabla\psi = 0.$$

Since $n = \nabla\psi/|\nabla\psi|$ we obtain

$$\frac{\partial\psi}{\partial s} + V|\nabla\psi| = 0.$$

This Hamilton-Jacobi equation is posed in the whole body Ω , and not only on the interface Σ , if the velocity V is known everywhere.

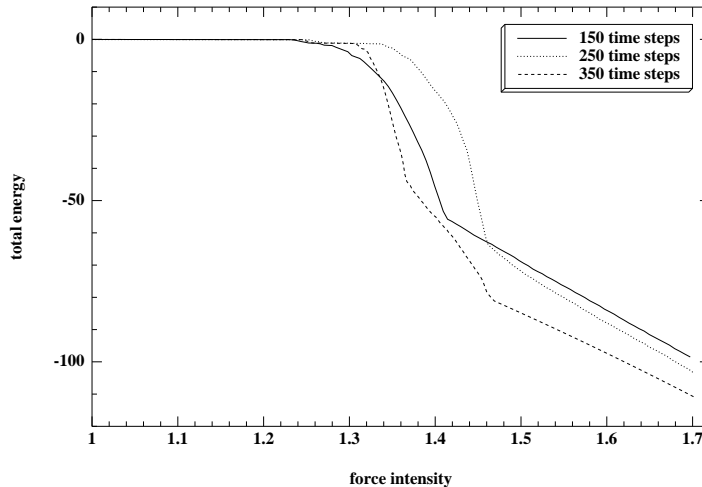


FIGURE 2. Mode I crack: total energy or cost function (7) versus force intensity for three different number of time steps (150, 250 and 350).

For the minimization of (7) we use the shape derivative

$$J'(\chi)(\theta) = \int_{\Sigma} v \theta \cdot n \, dS,$$

where the integrand v is given by Theorems 2.3 or 2.4. Since n and the state u_{χ} are defined everywhere in Ω , the integrand v in the shape derivative is defined throughout the domain Ω and not only on the interface Σ . Therefore, we can define a descent direction in the whole domain Ω by

$$\theta = -v n.$$

The normal component $\theta \cdot n = -v$ is therefore the advection velocity in the Hamilton-Jacobi equation

$$(14) \quad \frac{\partial \psi}{\partial s} - v |\nabla \psi| = 0.$$

Transporting ψ by (14) is equivalent to move the interface Σ (the zero level-set of ψ) along the descent gradient direction $-J'(\chi)$. Our proposed algorithm for the inner loop (ii) is an iterative method, structured as follows:

- (1) Initialization of the level set function ψ^0 as the signed distance to the previous damaged interface Σ_i corresponding to the characteristic function $\chi^0 \equiv \chi_i$.
- (2) Iteration until convergence, for $k \geq 0$:
 - (a) Computation of the state u_k by solving a problem of linear elasticity with coefficients A_{χ^k} .

- (b) Deformation of the interface by solving the transport Hamilton-Jacobi equation (14). The new interface Σ^{k+1} is characterized by the characteristic function χ^{k+1} or the level-set function ψ^{k+1} solution of (14) after a (pseudo-)time step Δs_k starting from the initial condition $\psi^k(x)$ with velocity $-v_k$ computed in terms of u_k . The (pseudo-)time step Δs_k is chosen such that $J(\chi^{k+1}) \leq J(\chi^k)$.
- (c) Irreversibility constraint: we replace χ^{k+1} by $\max(\chi^{k+1}, \chi^0)$ where $\chi^0 \equiv \chi_i$ corresponds to the damaged zone at the previous iteration of the outer loop (i).

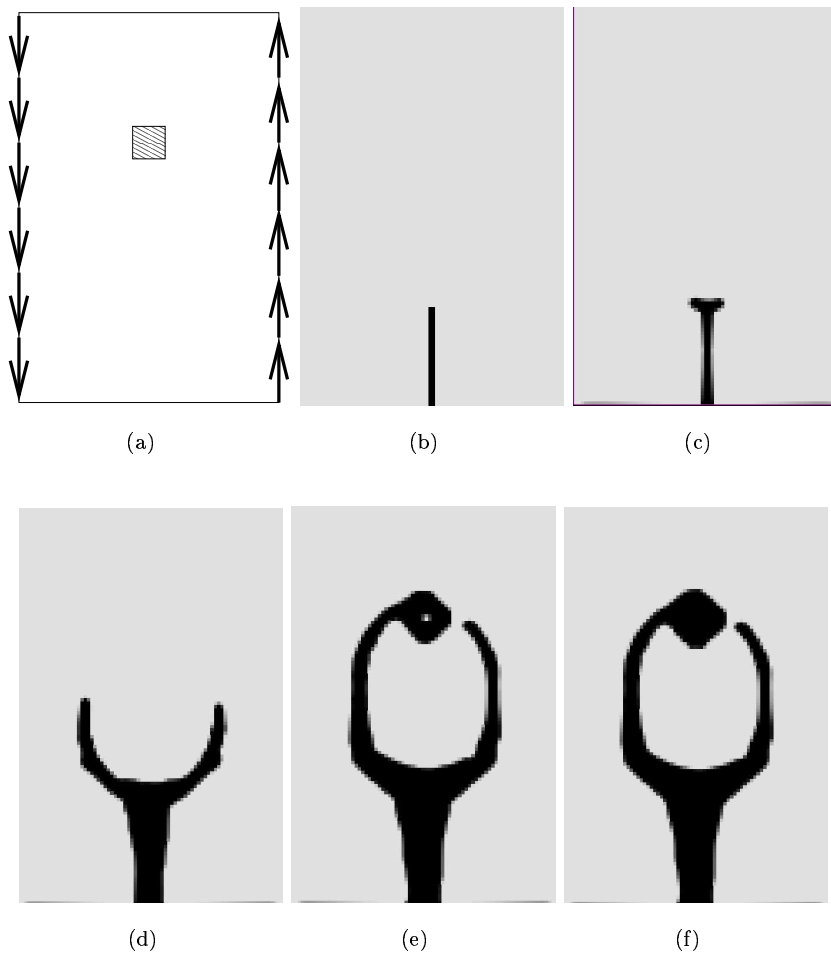


FIGURE 3. Mode II crack (coarse mesh): boundary conditions (a), initial crack (b). Cracks for a load intensity $g = 1$. (c), $g = 1.00015$ (d), $g = 1.0006$ (e), $g = 1.001$ (f).

From time to time, for stability reasons, we also reinitialize the level-set function ψ . The Hamilton-Jacobi equation (14) is solved by an explicit second order upwind scheme on a Cartesian grid. The boundary conditions for ψ are of Neumann type. Since this scheme is explicit in time, its (pseudo-)time step, given by a CFL condition is usually much smaller than Δs_k which plays the role of the descent step in the minimization of $J(\chi)$. Therefore, we run several explicit time steps of the Hamilton-Jacobi equation (14) between two evaluations of the displacement by standard Q1 finite elements.

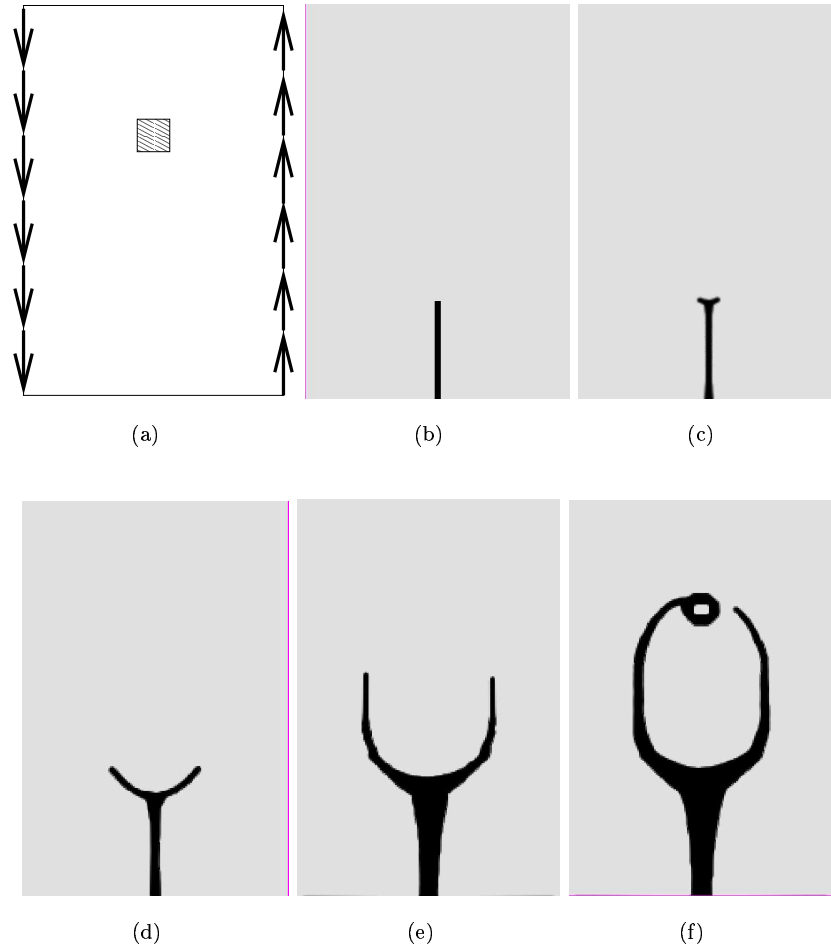


FIGURE 4. Mode II crack (fine mesh): boundary conditions (a), initial crack (b). Cracks for a load intensity $g = 1$. (c), $g = 1.00015$ (d), $g = 1.0006$ (e), $g = 1.001$ (f).

We now perform numerical experiments with a healthy material having Young's modulus $E = 10^4$ and Poisson ratio $\nu = 0.3$ (white in the pictures). The damaged phase is characterized by $E = 10$ and $\nu = 0.3$ (black in the pictures). With such a strong contrast between the two phases, the Francfort-Marigo damage model is

believe to behave almost like a brittle fracture model. Actually some models of fracture mechanics [16] are approximated by Γ -convergence techniques [10], [11], which is similar in spirit to a damage model. Our first tests are therefore on the simulation of plane crack propagation.

In Figure 1 we study a mode I crack on a rectangular mesh (80×120 cells). Uniform surface traction is applied on the vertical walls while the body is fixed on a small dark square (see Figure 1-(a)). The Griffith energy release rate is $\kappa = 10$. A vertical crack is initialized at the bottom (see Figure 1-(b)). We do not use the topological gradient in this case. The other pictures in Figure 1 correspond to an increasing magnitude of the applied traction (we use 150 time steps). We start from the initial crack with a force $g = 1$ and increase it progressively. We detect the first advance of the crack after 60 time steps leading to a force $g = 1.2348$ (see Figure 1-(c)). The last picture (h) in Figure 1, obtained at the 75th time step for a force intensity $g = 1.3074$, corresponds to the crack first reaching the top wall. Overall, we clearly see a crack propagating in straight line to the fixed square and then a non symmetric crack percolating to the top. The evolution of the total energy or cost function (7) as a function of the force intensity is displayed on Figure 2 for three different choices of the number of time steps (150, 250 and 350) with the same mesh. The abrupt decrease of the energy corresponds to the breakthrough of the crack on the top wall and thus the complete failure of the structure. For example, the last picture in Figure 1-(h) corresponds to a force intensity $g = 1.3074$ which lies in the rapidly decreasing zone of the cost function (for the curve of the 150 time steps test). The apparent plateau for small force intensities in Figure 2 is actually not flat: the crack stays at its initial position so the Griffith energy is constant but the potential elastic energy is decreasing quadratically with respect to the force intensity. However, the elastic energy is much smaller than the Griffith one so we cannot see any variation of the cost function except if we zoom on it.

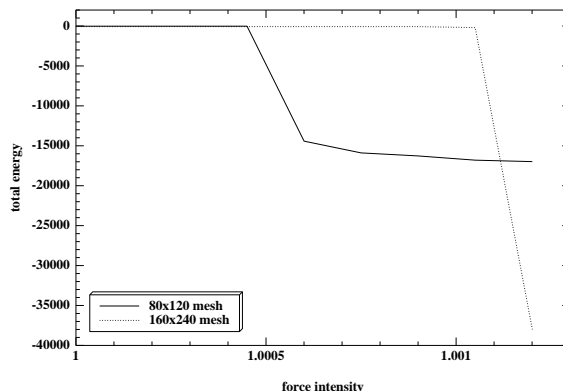


FIGURE 5. Mode II crack: total energy or cost function (7) versus force intensity for two different meshes.

We then simulate a mode II crack in Figure 3 for a coarse mesh (80×120 cells) and in Figure 4 for a finer mesh (160×240 cells). The Griffith energy release rate is now $\kappa = 0.0012$. A shear stress is applied on the vertical walls while the body is still fixed on a small dark square (see Figure 3-(a)). A vertical crack is initialized at the

bottom and we again do not use the topological gradient. We start from the initial crack with a force $g = 1$ which immediately yields an advanced of the crack, i.e., the crack moves at the first time step (see Figure 3-(c)). The remaining pictures are obtained after 4, 7 and 10 time steps respectively. We clearly have a crack branching in two symmetric branches. The same forces and the same time stepping is applied for both computations on the coarse and fine meshes. The computations seem to be reasonably mesh convergent in the sense that the same crack path is predicted. However, as can be checked on the evolution of the cost function (7) in Figure 5, the critical load which yields a sudden decrease of the energy (corresponding to the crack reaching the support of the body) is not the same. Further mesh refinements should be made for studying the convergence or not of this threshold. To study the influence of the contrast between the two phases, we keep the same Young's modulus for the healthy material, $E = 10^4$, but we change that of the damaged material to $E = 5 \cdot 10^3$. We run the same experiment on the coarse mesh (with a different value of the Griffith energy release rate κ) and we obtain a thick damaged zone which does not look like a crack anymore, see Figure 6.

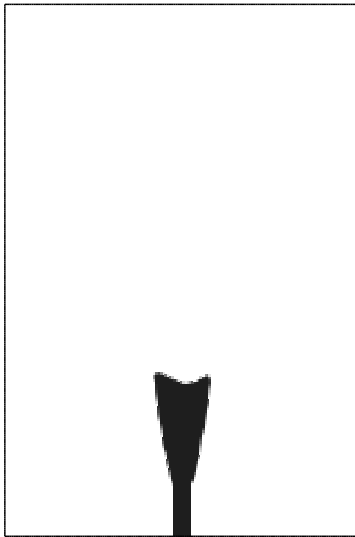


FIGURE 6. Mode II crack: thick damaged zone for a 1 to 2 contrast between the phases.

The next example is an L-shaped structure (see Figure 7) which is intended to show how the topological gradient can be used. While the previous test cases were initialized with a pre-existing crack, the L-shape example has no such initialization. Instead, we use the topological gradient at the first time step to decide if it is worth to nucleate a small hole and where it should be. Remark that the topological gradient used here (as described in Section 3) is based on a small hole cut inside the bulk of a structure. A different type of topological gradient should be defined for a hole biting the boundary of the structure. Nevertheless, we employ the same topological gradient everywhere inside and at the boundary of the structure. More precisely, starting from an initial domain without any crack or damaged zone, we use the topological gradient at the first time step to nucleate a small (one cell)

damaged area. In subsequent time steps we do not use anymore the topological gradient and just rely on the shape gradient for evolving the interface. The L-shape is clamped at the top wall and a force is acting on the middle of its right wall (see Figure 7-(a)). It is meshed with 6400 cells, the initial force is $g = 1$, and 10 time steps are performed. The Griffith energy release rate is $\kappa = 5$. The topological gradient nucleates a damaged zone at the reentrant corner as expected (see Figure 7-(b)). Then a crack starts running until it cuts the body at the 10th time step.

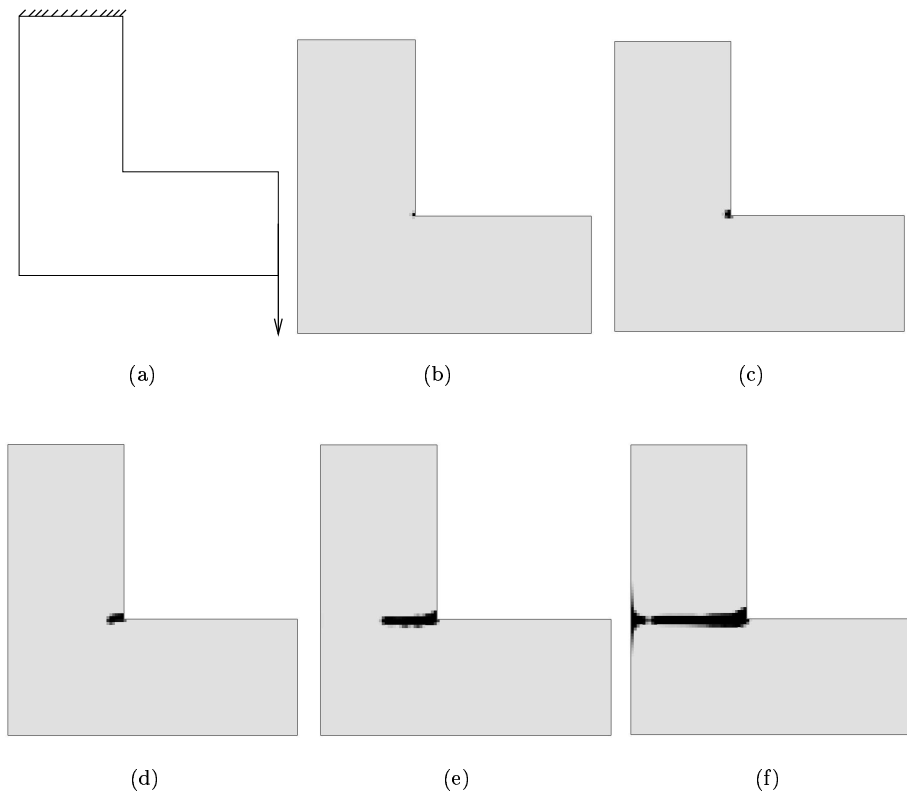


FIGURE 7. L-shape: boundary conditions (a), initial damaged zone obtained by the topological gradient (b). Cracks for a load intensity $g = 1.5625$ (c), $g = 1.9531$ (d), $g = 2.4414$ (e), $g = 3.0518$ (f).

Eventually we consider a 3-d test case: a beam which is simply supported at its two lower extremities and is vertically loaded on the center of its top face. The healthy phase has now Young's modulus $E = 1$, and Poisson ratio $\nu = 0.3$ while the damaged phase is characterized by $E = 0.3$ and $\nu = 0.3$. By symmetry only one fourth of the domain is meshed with 16800 rectangular cells. The Griffith energy release rate is $\kappa = 250$. Starting from a unit force, at each time step it is multiplied by a factor 1.0488. On Figure 8 we plot the isosurfaces of the healthy domain after 1, 5, 10, 15, 20 and 25 time steps (the beam is deformed according to the elastic displacement).

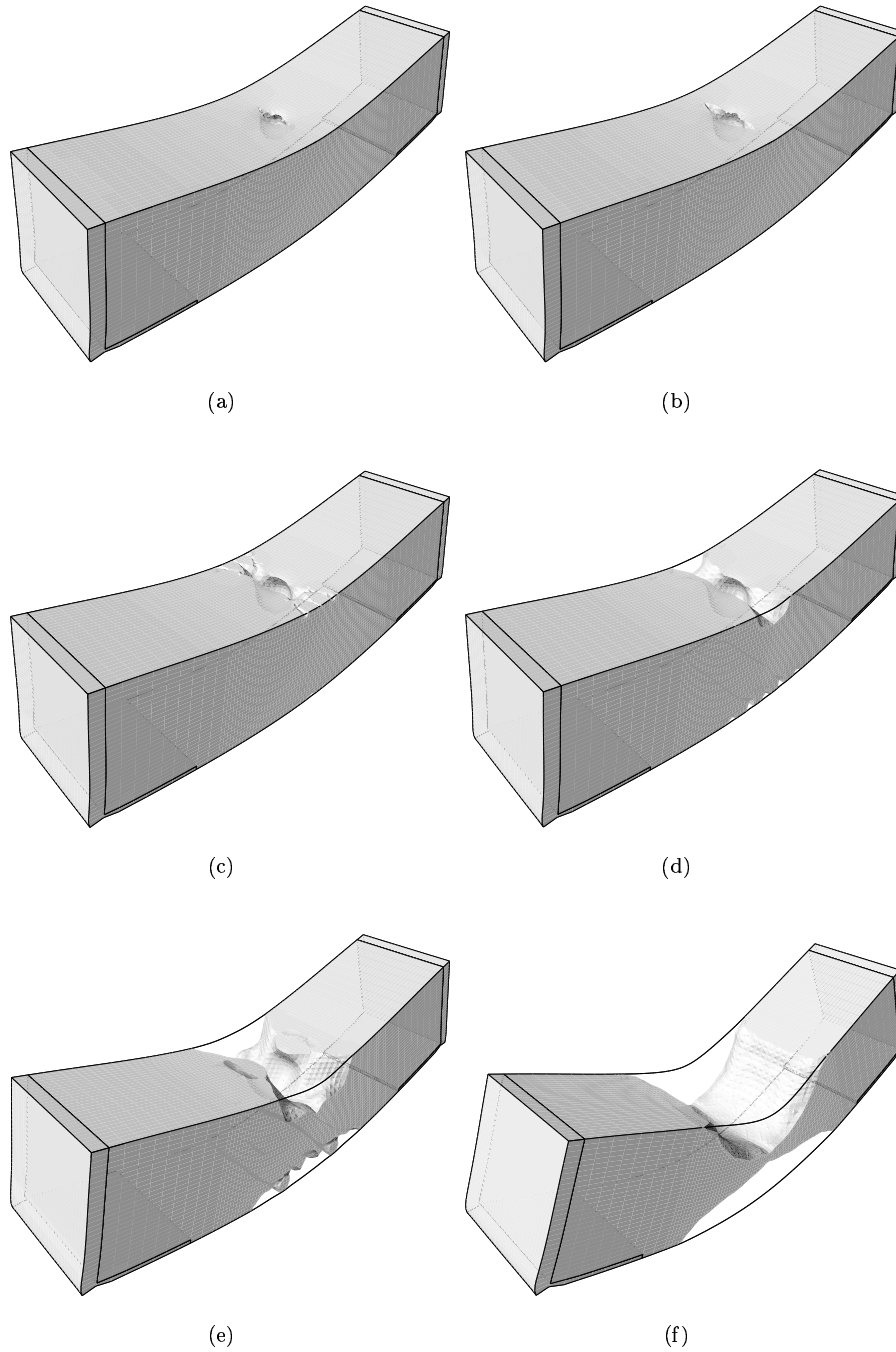


FIGURE 8. Simply supported beam. Damage evolution for a load intensity $g = 1$. (a), $g = 1.27$ (b), $g = 1.61$ (c), $g = 2.04$ (d), $g = 2.60$ (e), $g = 3.30$ (f).

5. CONCLUSION

We have proposed a numerical implementation of the Francfort-Marigo model of brittle damage evolution. It is based on the notion of shape derivative and topological gradient in the context of the level set method. By using a simple gradient algorithm for the minimization of the total energy we compute local minimizers which may be physically more sound than global minimizers. Our algorithm has been implemented and tested in two and three dimensions. For a large contrast between the healthy and damaged phases our numerical simulations show that the Francfort-Marigo damage model is able to simulate crack propagations. Although the minimization of the total energy (7) is not a well-posed problem in the sense that it usually admits no global minimizer (see [15]), our numerical approach seems to be stable. We did not experience any instabilities (oscillations or fingering of the interface) and our first results are reasonably mesh convergent. If required, stability could certainly be achieved by adding a perimeter constraint, i.e., adding a surface energy term (proportional to the area of the interface) to (7).

Much remain to be done. We need to investigate in greater details the issues of convergence under mesh and/or time step refinement. We plan to make comparisons with previous results [2] based on global minimization and a relaxed formulation of the model. We will also investigate the connections with models of brittle fracture approximated by Γ -convergence techniques [10], [11], which are similar in spirit to a damage model. Eventually we shall try to reproduce physical experiments. These issues, as well as many other technical points, will be the focus of our next work [5].

REFERENCES

- [1] Allaire, G., *Conception optimale de structures*, Mathématiques et Applications, Vol. 58, Springer (2007).
- [2] Allaire, G., Aubry, S., Jouve, F., Simulation numérique de l'endommagement à l'aide du modèle Francfort-Marigo, in Actes du 29ème congrès d'analyse numérique, *ESAIM Proceedings*, **3**, pp.1-9 (1998).
- [3] Allaire, G., Jouve, F., Toader, A.-M., Structural optimization using sensitivity analysis and a level-set method, *J. Comput. Phys.* **194** (1), 363-393, (2004).
- [4] Allaire, G., Jouve, F., de Gournay, F., Toader, A.-M., Structural optimization using topological and shape sensitivity via a level set method, *Control and Cybernetics* **34**, 59-80 (2005).
- [5] Allaire, G., Jouve, F., Van Geothem, N., Damage evolution in brittle materials by shape and topological sensitivity analysis, in preparation.
- [6] Ammari, H., *Introduction to mathematics of emerging biomedical imaging*, Mathématiques et Applications, Springer Verlag, to appear.
- [7] Ammari, H., Kang, H., *Reconstruction of small inhomogeneities from boundary measurements*, Lecture notes in mathematics, 1846. Springer, (2000).
- [8] Ammari H., Kang H., Nakamura G., Tanuma K., Complete asymptotic expansions of solutions of the system of elastostatics in the presence of an inclusion of small diameter and detection of an inclusion, *J. Elasticity* **67**, no. 2, 97-129 (2002).
- [9] Bernardi, Ch., Pironneau, O., Sensitivity of Darcy's law to discontinuities. *Chinese Ann. Math. Ser. B* **24**, no. 2, 205-214 (2003).
- [10] Bourdin, B., Francfort, G. A., Marigo, J.-J., Numerical experiments in revisited brittle fracture. *J. Mech. Phys. Solids* **48**, no. 4, 797-826 (2000).
- [11] Bourdin, B., Francfort, G. A., Marigo, J.-J., The variational approach to fracture, *Journal of Elasticity*, in press.
- [12] Burger, M., Hackl, B., Ring, W., Incorporating topological derivatives into level set methods, *J. Comp. Phys.*, **194** 1, 344-362 (2004).

- [13] Eschenauer, H., Kobelev, V., Schumacher, A., Bubble method for topology and shape optimization of structures, *Structural Optimization*, **8**, 42–51 (1994).
- [14] Francfort, G., Garroni, A., A variational view of brittle damage evolution, *Arch. Ration. Mech. Anal.* **182**, no. 1, 125–152 (2006).
- [15] Francfort, G., Marigo, J.-J., Stable damage evolution in a brittle continuous medium, *Eur. J. Mech., A/Solids*, **12** (2), 149-189 (1993).
- [16] Francfort, G., Marigo, J.-J., Revisiting brittle fracture as an energy minimization problem, *J. Mech. Phys. Solids*, **46** (8), 1319-1342 (1998).
- [17] Garreau, S., Guillaume, P., Masmoudi, M., The topological asymptotic for PDE systems: the elasticity case. *SIAM J. Control Optim.* **39**, no. 6, 1756–1778 (2001).
- [18] Garroni, A., Larsen, C., Threshold-based Quasi-static Brittle Damage Evolution, preprint.
- [19] Henrot, A., Pierre, M., *Variation et optimisation de formes*, Mathématiques et Applications, Springer Verlag, (2005)
- [20] Hettlich, F., Rundell, W., The determination of a discontinuity in a conductivity from a single boundary measurement. *Inverse Problems*, **14**, no. 1, 67–82 (1998).
- [21] Osher, S., Sethian, J.A., Front propagating with curvature dependent speed: algorithms based on Hamilton-Jacobi formulations. *J. Comp. Phys.* **78**, 12-49 (1988).
- [22] Pantz, O., Sensibilité de l'équation de la chaleur aux sauts de conductivité, *C. R. Acad. Sci. Paris, Ser. I* **341**, 333-337, (2005).
- [23] Sokołowski, J., Żochowski, A., On the topological derivative in shape optimization, *SIAM J. Control Optim.*, **37**, 1251–1272 (1999).
- [24] Wang, M.Y., Wang, X., Guo, D., A level set method for structural topology optimization, *Comput. Methods Appl. Mech. Engrg.*, **192**, 227–246 (2003).
- [25] Wang, X., Yulin, M., Wang, M.Y., Incorporating topological derivatives into level set methods for structural topology optimization, in *Optimal shape design and modeling*, T. Lewinski et al. eds., 145–157, Polish Academy of Sciences, Warsaw (2004).